A High Resolution Study of Non-Reacting Fuel Sprays using Large-Eddy Simulations

A. Wehrfritz*, V. Vuorinen, O. Kaario, M. Larmi
Department of Energy Technology, Aalto University, Finland
armin.wehrfritz@aalto.fi

Abstract

The present study deals with Large-Eddy Simulations (LES) of non-reacting fuel sprays in internal combustion engine like conditions. The main objective is to investigate the influence of the grid size on droplet breakup and evaporation in conjunction with the implicit LES method for the well defined reference case "Spray A". A sufficient agreement with the experimental results concerning liquid and vapor penetration was found for the two highest mesh resolutions. The coarsest mesh could not capture the turbulent transition correctly and thus over-predicted liquid and vapor penetration. Both investigated breakup models performed reasonable well, even though differences in predicted droplet size were found. The differences in droplet size affect again the global spray quantities (liquid/ vapor penetration). Hence, a further investigation and tuning of the breakup model parameter is suggested for the chosen LES approach.

Introduction

Sprays have a fundamental role in internal combustion engine applications. As the automotive industry is driven by the demand for lower emissions and higher fuel efficiency, fuel sprays become important in combustion optimization. Particularly, a deeper understanding of the processes and phenomena related to the liquid–gas phase interaction is crucial, as it is the first step in the mixture formation. Beside experimental studies, 3D flow simulations offer a versatile tool to investigate these processes in detail. However, the methods and models used in such simulations impose their own challenges, especially with an increasing degree of detail.

Traditionally, Computational Fluid Dynamic (CFD) simulations of turbulent flows have been carried out using the Reynolds-Averaged Navier-Stokes (RANS) approach. In RANS simulations all scales of turbulence are modeled and the results can be seen as a time averaged description of the flow field. To simulate directly the large scales of turbulence rather than model them gives a higher degree of detail and allows a more advanced analysis of the physical problem. These so called Large Eddy Simulation (LES) are computationally significantly heavier, but became affordable also for engineering applications with the recent progress in computational power. Whereas LES still demands the modeling of the small, usually sub-grid, scales Direct Numerical Simulation (DNS) resolves the whole turbulence spectrum directly and delivers therefore the most accurate results. However, the accuracy of DNS comes with a very high computational cost and is therefore barely affordable for non-fundamental research.

The main computational concepts for spray simulations are the Lagrangian Particle Tracking (LPT) and the Euler-Euler (E-E) method. Where the latter treats both the gaseous and liquid phase as continua, the LPT method assumes the liquid phase as discreet particles. The E-E method is well suited for dense sprays as they occur in the near nozzle region of typical fuel sprays, but becomes unpractical in more dilute spray regions where again the LPT is better suited. As typical fuel sprays are characterized by a very short liquid core and fast atomization (i.e. primary breakup) the sprays become quickly dilute and hence the LPT method is commonly used for fuel-spray simulations.

In the present study spray simulations are carried out using the LES and LPT methods. As the LES method in general demands a higher mesh resolution, the cell size may reach a critical limit for certain spray sub-models. This study presents a comparison of two droplet breakup models for different mesh sizes. The investigate breakup models are the Enhanced Taylor Analogy Break-up (ETAB) [1, 2] and the Kelvin-Helmholtz Rayleigh-Taylor (KHRT) [3] model. The results are validated against the experimentally well investigated non-reacting "Spray A" [4] test case as defined by the Engine Combustion Network (ECN). The background motivation for the study is to explore the limitations, possibilities and challenges that come with the LPT method in high resolution LES. Furthermore, the study lays a foundation for reacting spray simulations using the LES method, where the decrease in cell size becomes even more important.

*Corresponding author: armin.wehrfritz@aalto.fi

Governing equations

Navier-Stokes equations

The equations solved to describe the flow field of the continuous gas phase are the compressible Navier-Stokes (NS) equations. The set of equations describing the conservation of mass 1, momentum 2 and energy 3 is supplemented by transport equations for the species mass fractions of the gas composition. The equations read

$$\frac{\partial \rho}{\partial t} + \frac{\partial \rho u_j}{\partial x_j} = S_m \tag{1}$$

$$\frac{\partial \rho u_i}{\partial t} + \frac{\partial \left(\rho u_i u_j\right)}{\partial x_j} = \frac{\partial}{\partial x_j}\left(-p\delta_{ij} + \sigma_{ij}\right) + S_i \tag{2}$$

$$\frac{\partial \rho h}{\partial t} + \frac{\partial (\rho h u_j)}{\partial x_j} = \frac{\partial p}{\partial t} + u_j \frac{\partial p}{\partial x_j} + \frac{\partial}{\partial x_j}\left(\lambda \frac{\partial T}{\partial x_j}\right) + S_h \ , \tag{3}$$

where ρ, u_i, h, T and p denote the density, velocity component in x_i direction, enthalpy, temperature and pressure, respectively. The heat conductivity is given by λ and the viscous stress tensor in equation 2 is defined as

$$\sigma_{ij} = \mu\left(\frac{\partial u_i}{\partial x_j} + \frac{\partial u_j}{\partial x_i} - \frac{2}{3}\frac{\partial u_i}{\partial x_j}\delta_{ij}\right), \tag{4}$$

where μ is the dynamic viscosity of the fluid. Each equation contains a source term for mass (S_m), momentum (S_i) and energy (S_h) that incorporates the interaction of the continuous (gas) with the dispersed (liquid) phase.

Droplet kinematics, mass and heat transfer

Following the LPT approach, the liquid phase is described by several equations for droplet motion, heat and mass transfer. By defining the droplet Reynolds number

$$Re_d = \frac{|\boldsymbol{u}_g - \boldsymbol{u}_d|\, d_d \rho_g}{\mu_g}$$

and the droplet time scale

$$\tau_d = \frac{\rho_d {d_d}^2}{18 \rho_g \mu_g} \tag{5}$$

the equation of motion reads

$$\frac{d}{dt}\boldsymbol{u}_d = \frac{C_D}{\tau_d}\frac{Re_d}{24}\left(\boldsymbol{u}_g - \boldsymbol{u}_d\right) \ , \tag{6}$$

where the subscript d denotes the droplet and g the gas phase quantities. The empirically determined values for the drag coefficient C_D can be expressed by the relations

$$C_D = \begin{cases} \dfrac{24}{Re_d}\left(1 + \dfrac{1}{6}{Re_d}^{2/3}\right) & Re_d < 1000 \\ 0.424 & Re_d \geq 1000 \end{cases} .$$

The change in droplet position is than obtained from

$$\frac{d}{dt}\boldsymbol{x}_d = \boldsymbol{u}_d \ .$$

The mass transfer from liquid to gas phase is modeled according to the droplet vaporization correlation by Frössling and hence the change in droplet mass can be expressed by $\dfrac{dm_d}{dt} = \dfrac{m_d}{\tau_e}$ with the the evaporation time scale

$$\tau_e = \frac{\rho_d {d_d}^2}{6 D_m \, Sh \, \rho_v \ln\left(\frac{p - p_{v,\inf}}{p - p_{v,s}}\right)} \ . \tag{7}$$

The heat transfer at the droplet surface is derived from the droplet energy balance and the Ranz-Marshall correlations for Sherwood (Sh) and Nusselt (Nu) number [5, 6] are applied in the equations for mass and heat transfer.

The implementation of the LPT method in OpenFOAM incorporates the parcel approach, which groups physically similar droplets into a parcel and reduces therefore the computational cost significantly.

Droplet breakup

The advantages and disadvantages of droplet breakup modeling have been previously described by Vuorinen et al. [7], who proposed a simplified model to take into account the droplet breakup at lower Weber numbers. Here, we however study some of the standard models in order to further investigate how the KHRT and the ETAB models perform in implicit LES.

The KHRT model was first proposed by Reitz [3] and is a combination of the Kelvin-Helmholtz (KH) wave model and the assumption of occurring Rayleigh-Taylor (RT) instabilities at the droplet surface. The KH breakup mechanism assumes the droplets to behave like a liquid jet injected into an incompressible gas environment. The liquid surface is therefore subject to small perturbations that are amplified by the liquid–gas phase interaction which leads to small droplets stripped off from the surface. Based on the perturbation growth rate Ω_{KH} and wavelength Λ_{KH} a breakup time and droplet diameter can be determined. Reitz gives correlation obtained from curve-fits to the analytical solution for the wavelength and growth rate and the breakup time is than given by

$$\tau_{_{KH}} = 3.726\ B_1 \frac{r}{\Lambda_{KH}\Omega_{KH}}\ , \tag{8}$$

where r denotes the radius of the initial droplets. The RT model is based on theoretical considerations on the stability of liquid–gas interfaces that are accelerated in normal direction. Assuming a linear disturbance growth a growth rate and wavelength can be determined. The breakup time is than obtained by the reciprocal of the growth rate and a correction factor C_τ to delay the breakup under certain conditions as

$$\tau_{_{RT}} = C_\tau \frac{1}{\Omega_{RT}}\ . \tag{9}$$

Droplet breakup is encountered if $d_d > \Lambda_{RT}$ and τ_{RT} is greater than the time of disturbance growth. Both mechanisms, KH and RT, are implemented in a competing manner to determine the droplet breakup.

As the ETAB model is based on the TAB (Taylor Analogy Break-up) model proposed by O'Rourke and Amsden [8], they both share the basic concept for calculating the breakup time. Following the Taylor Analogy, the droplet distortion $y = \dfrac{2x}{r}$, where r is the droplet radius and x the deviation of the droplet equator, can be modeled as a one dimensional, forced, damped, harmonic oscillator. Hence the equation of motion reads

$$\ddot{y} + \frac{5\mu_d}{\rho_d r^2}\dot{y} + \frac{8\sigma}{\rho_d r^3} y = \frac{2\rho_g \left(\boldsymbol{u_d} - \boldsymbol{u_g}\right)^2}{3\rho_d r^2}\ . \tag{10}$$

A solution to the equation 10 leads to an expression for the distortion y and the droplets are assumed to breakup if y exceeds unity and thus a breakup time can be calculated. In the original TAB model the radius of the child droplets after breakup is based on an energy balance of the surface and oscillation energy of the parent droplet and the surface and kinetic energy of the child droplet. The ETAB model [1, 2] is a modified version of the TAB model, which aims to predict more realistic results for global spray parameters. Tanner therefor proposed a new method for calculating the number and size of the child droplets after breakup, which assumes the rate of child droplet generation to be proportional to the number of droplets. The proportional constant depends on the breakup regime, which is characterized by the Weber number

$$We = \frac{\rho_g r (\boldsymbol{u}_g - \boldsymbol{u}_d)^2}{\sigma}\ . \tag{11}$$

In general the ETAB model computes a greater child radius and results therefor in a more realistic droplet size distribution, especially in the dense spray region close to the nozzle orifice.

Both models include certain constants that are adjusted to match experimental droplet sizes and breakup rates. These empirical constants are well tested in a vast amount of simulations, where the majority is based on the RANS approach. RANS simulations are usually carried out with fairly large cell sizes (characteristic length of about 500μm), e.g. [1–3, 9–11] and the models received little testing with cell sizes suitable for LES as it was also found by Bharadwaj and Rutland [12]. For a detailed description of these constants it is referred to the original publications by Reitz [3] and Tanner [1]. In this study the model constants are set to their default value as listed in Table 1 and 2.

Simulation setup and Geometry

The simulations in the present paper are carried out for the Spray A test conditions. The ambient gas density and temperature for Spray A are 22.8 kg/m3 and 900 K, respectively. For the non-reacting setup the gas composition in the test vessel consists of 100% nitrogen. The injected fuel is n-dodecane (C12H26) in order to resemble a

Table 1. KHRT model constants

B_0	B_1	C_τ	C_{RT}	ms_{Limit}	We_{Limit}
0.61	40	1	0.1	0.03	6

Table 2. ETAB model constants

C_μ	C_Ω	We_{Crit}	k_1	k_2	$We_{Transition}$
10	8	12	0.2	0.2	100

diesel-like fuel spray and the nominal injection pressure is 150 MPa. The nominal nozzle diameter of the injector is 90 μm, and the discharge coefficient was experimentally determined as 0.86, which leads to an averaged injection velocity of approximately 590 m/s.

The simulations are carried out using the open source CFD tool box OpenFOAM [13]. The simulation approach is based on a compressible flow solver with an implicit pressure treatment based on the PISO-algorithm. The spatial accuracy of the code is formally 2nd order and an implicit, 2nd order accurate time integration is used. The turbulence modeling approach is based on the assumption that the grid, or more precisely the numerical discretisation scheme, functions as an implicit low-pass filter and it is assumed that sub-filter scales will dissipate in the same manner as the numerical scheme. Hence, the unresolved turbulence scales are not modeled explicitly, which is commonly referred to as implicit or no-model LES [14].

The geometry of the computational domain resembles the combustion vessel at the Sandia National Laboratory, USA for which the experimental validation data are obtained. A fully hexahedral base mesh is used, which is refined by a 2:1 cell-splitting approach in the spray region in order to obtain appropriate cell sizes for LES. Three mesh sizes are simulated in this study, where the mesh with the highest refinement level leads to a minimum cell size of 62.5 μm and approximately 4.6 million cells. The cell count for the intermediate and coarse mesh is 1.2 and 0.8 million. The computational meshes are shown in Figure 1, where the colors in the first sub-figures (a-c) correspond to the refinement level and the sub-figure (d) shows a wireframe representation of the mesh. It shall be noted that the figures show only the refinement regions. The coarsest refinement region (500 μm) extend to 52 mm from the injection location and the 250 μm region to 50 mm for all meshes, where the length of the computational domain in injection direction is 108 mm. In the meshes with a minimum cell size of 125 μm and 62.5 μm the finest region extends to 25 mm, where in the 62.5 μm mesh the transition layer around the 62.5 μm region extends to 26 mm. The injection mass flow rate for the present simulations corresponds to the experimental profile measured at

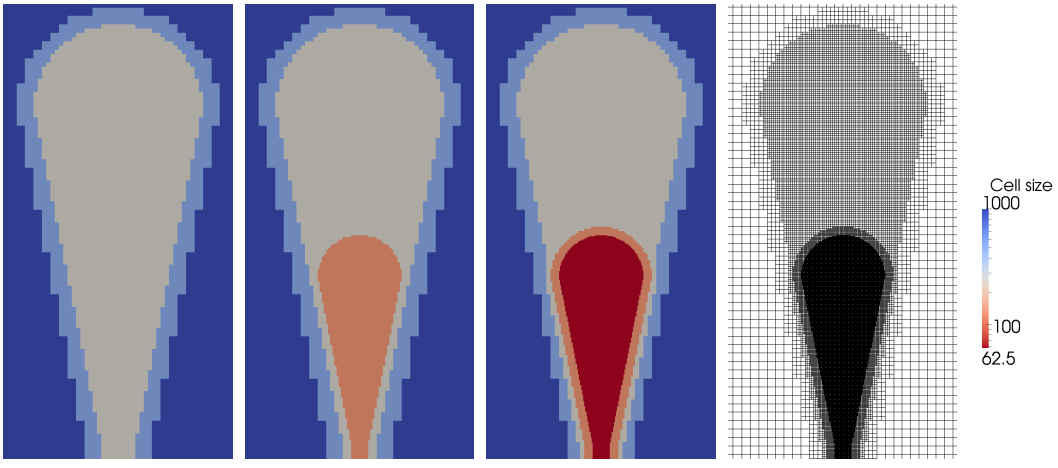

(a) 250μm (b) 125μm (c) 62.5μm (d) Wireframe

Figure 1. Refinement regions for the computational meshes with a minimum cell size of (a) 250 μm, (b) 125 μm and (c) 62.5 μm. Figure (d) shows a wireframe representation of the finest mesh.

the Sandia National Laboratory, USA [4]. The present setup does not cover the direct simulation of atomization processes by an explicit atomization model. Typical atomization models share the idea of injecting "blobs" of the size of the nozzle hole that resemble the injection of a liquid core. Specific mechanisms are than used to strip-off smaller droplets from these blobs or break them up. Since the cell sizes of the two finest meshes are close to or even smaller than the nozzle hole diameter, the big "blobs" would violate some basic assumptions of the LPT approach as the ratio of liquid to gas volume would be close to or even exceed unity. Hence, the atomization was accounted

Table 3. Rosin-Rammler distribution parameter

D_{max}	D_{min}	d	n
18 μm	1 μm	6 μm	3

for by an Initial Droplet Size Distribution (IDSD) and the injection location can be considered to be downstream from the original injector. Thus, also a bigger injector diameter of 450 μm was applied and the actual injection location for each droplet was determined by a box-sampling method. This method has been shown to work well for LES spray simulations as e.g. in [7] A Rosin-Rammler IDSD with the parameter as listed in Table 3 was chosen for all simulations. The IDSD parameter lead to an initial Sauter Mean Diameter (SMD) of approximately 6 μm. The small initial SMD is an estimate considering the shifted injection location and increased injection diameter. The high injection velocity and hence the low droplet relaxation time τ_d (equation 5) in combination with the small cell sizes require a small time step which was set to $dt = 2 \cdot 10^{-8}$s for all simulations.

Results and Discussion

Spray visualization

The instantaneous spray vapor mass fraction is visualized in Figure 2 by snapshots at time $t = 0.5$ ms. For each simulated mesh size instantaneous snapshots comparing the ETAB (left) and KHRT (right) model are shown. As expected, the plots with an increased mesh resolution give a more detailed description of the flow field, where the increase to a cell size of 125 μm is already sufficient enough to indicate the entrainment of the surrounding gas. Finally the 62.5 μm mesh is able to show growing Kelvin-Helmholtz waves at the vapor–ambient gas interface. However, it is apparent that the results for the vapor mass fraction differ not only between the two breakup models,

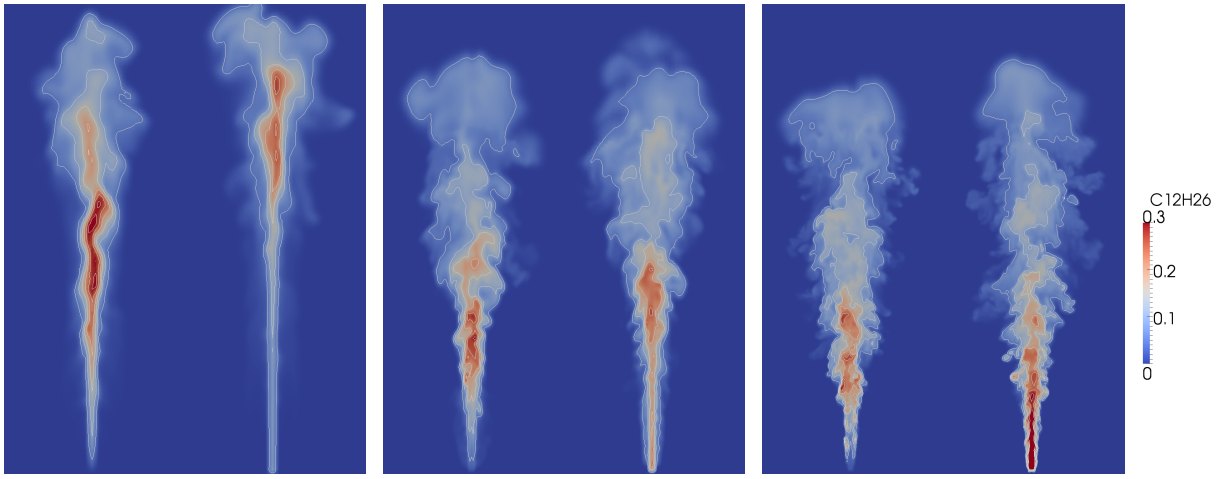

(a) 250μm (b) 125μm (c) 62.5μm

Figure 2. Instantaneous vapor mass fraction at time $t = 0.5$ ms for three mesh sizes (250 μm, 125 μm and 62.5 μm) comparing the ETAB (left) and KHRT (right) breakup model.

but show also significant differences, especially in magnitude, with a decreasing cell size.

Liquid and vapor penetration

In the following global spray quantities are analyzed to further investigate these differences. As one of the two essential quantities in non-reacting sprays, the liquid penetration over time for the six simulated cases is compared to the experimental data obtained at the Sandia National Laboratory in Figure 3. In the present study, the liquid penetration is defined as the maximum distance of 95% liquid mass to the injection location. As a first observation it can be concluded that the mesh with a 250 μm cell size is neither with the ETAB nor with the KHRT model able to predict the liquid penetration correctly for the present simulation setup. The cell size is too large to model the momentum transfer from liquid to gas phase correctly and to capture the turbulent motion of the flow. The

situation improves significantly with a cell size of 125 μm in the main spray region, which leads in the case of the ETAB model to an accurate prediction of the liquid penetration as it is also observed for the finest mesh. For the KHRT model, the simulations with a 125 μm overshoot by approximately 5mm and only the 62.5 μm mesh delivers acceptable results. Figure 4 shows the vapor penetration for the simulated cases, which is defined as the

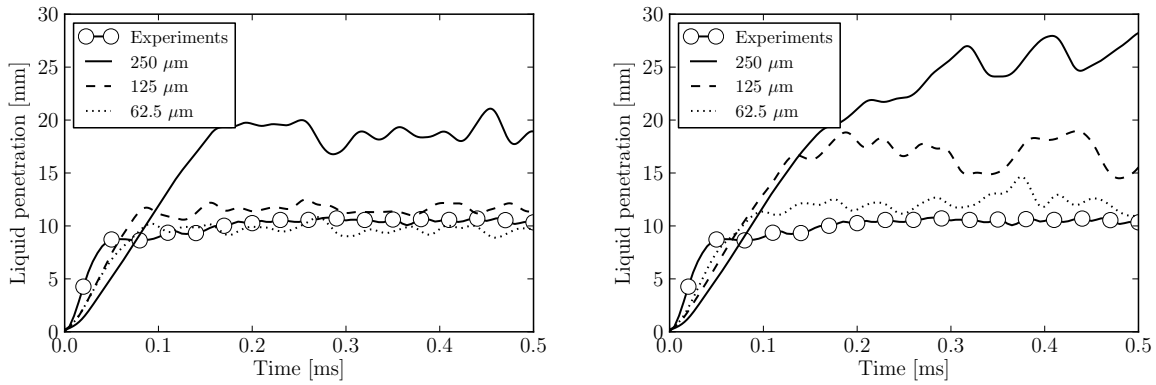

(a) ETAB (b) KHRT

Figure 3. Liquid penetration over time for the three mesh sizes comparing the ETAB and KHRT breakup model.

the maximum distance of 0.001 vapor mass fraction to the injection location. The results for the vapor penetration are in a better agreement with the experimental data. However, the 250 μm cell size is still found to over-predict the vapor penetration as the transition to a fully turbulent jet is not captured. It is also observed that for both breakup models the 62.5 μm mesh under-predicts the vapor penetration.

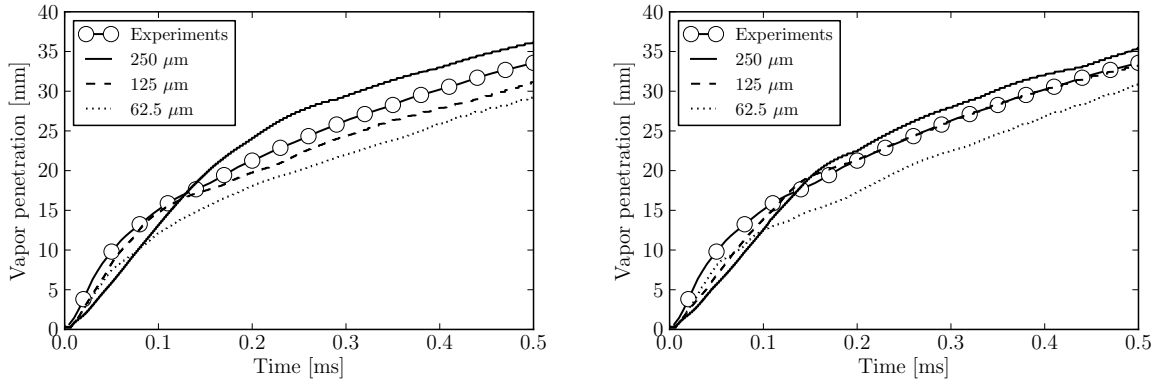

(a) ETAB (b) KHRT

Figure 4. Vapor penetration over time for the three mesh sizes comparing the ETAB and KHRT breakup model.

Droplet diameter and evaporation

As for the cases with equal mesh sizes only the breakup model was changed, an analysis of the droplet diameter is done. Therefore the Sauter Mean Diameter (SMD) calculated in 0.2 mm intervals along the injection normal direction z is plotted in Figure 5. For the ETAB model a constant SMD $\approx 0.35\mu$m along the z-direction is found for all mesh sizes. Contrary to the ETAB model the KHRT model has not only significantly higher values for the SMD, but also differences depending on the mesh size. Where for the meshes with a cell size of 250 and 125 μm an almost constant SMD of approximately 1.5 μm is observed, the mesh with the minimum cell size of 62.5 μm predicts a lower SMD of approximately 1.1 μm. In order to further analyze the under-predicted vapor penetration,

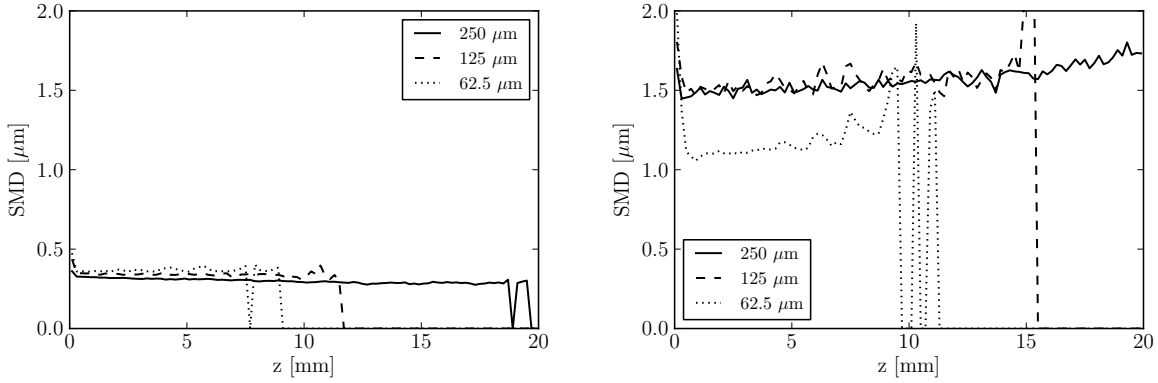

(a) ETAB (b) KHRT

Figure 5. Sauter Mean Diameter (SMD) in 0.2 mm intervals along injection normal direction z for the three mesh sizes and two breakup models at time $t = 0.5$ms.

the vapor mass fraction along the spray-centerline is plotted in Figure 6. For the simulations with the ETAB model, the vapor mass fraction behaves as expected from the SMD data. An initial increase of the vapor mass fraction along the centerline is observed until the maximum liquid penetration is reached, followed by a decrease. The decrease stems from the increasing turbulent motion and hence the spread in radial direction, as it is also seen in Figure 2. The results for the KHRT model are significantly different, as for all three mesh sizes a steep rise is observed close to the injection location. The maximum value of this initial rise is consistently increasing with the mesh resolution and is suspected to be attributed to pressure fluctuations in combination with the larger droplet sizes. These pressure fluctuations, may result in a higher evaporation rate in the near nozzle region and hence reduce the vapor penetration. However, within the scope of this study it was not possible to analyze this behavior in detail as an accurate modeling of the near nozzle region in combination with an advanced pressure treatment would be necessary to further investigate these phenomena.

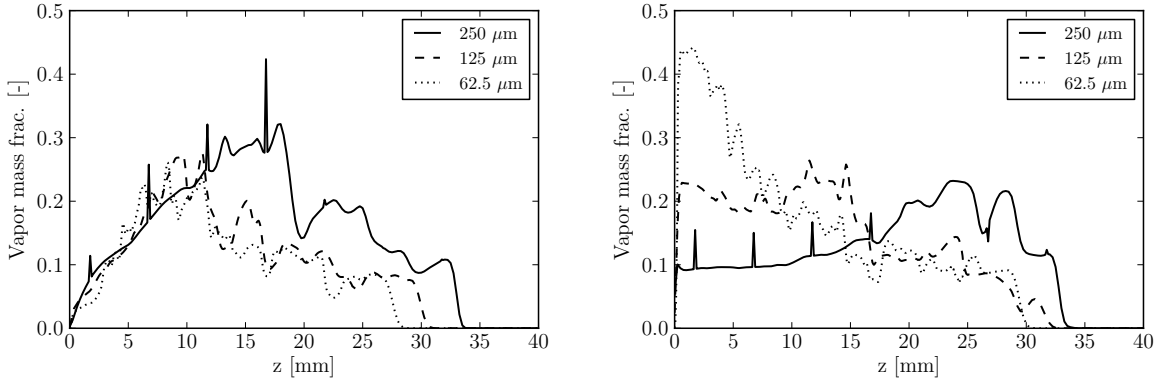

(a) ETAB (b) KHRT

Figure 6. Vapor mass fraction along the injection normal direction z for the three mesh sizes and two breakup models at time $t = 0.5$ms.

Conclusions

In the present study simulations using the LES method for the Spray A test case were carried out. A comparison of two breakup models on three mesh resolutions was made. It was found that a mesh size of 250 μm is not

sufficient enough to resolve the transition towards the fully turbulent motion of the spray for the given simulation setup. However, simulations with a mesh resolution of 125 μm showed already reasonable results.

A further increase in resolution led to a better prediction of the liquid penetration but revealed possible limits of the given simulation approach as unphysical pressure fluctuations in combination with larger droplets might cause a higher evaporation rate in the near nozzle region. Hence, an improvement for further studies could be a more accurate modeling of the injection process and an improved pressure treatment, especially concerning the high injection velocities.

Keeping in mind that the default breakup model parameter, as they were used in the present study, were obtained for specific spray conditions and mainly tuned with respect to RANS simulations an adjustment might further improve the results. Also the simplified breakup model recently proposed by Vuorinen et al. [7] is expected to improve the results significantly as it was shown to model consistently the sensitivity of breakup rate to Stokes number St. Since Stokes number ($St \sim {d_d}^2$) and the evaporation time scale ($\tau_e \sim {d_d}^2$) show both the same proportionality to the square of the droplet diameter, further improvements in evaporation rate and vapor penetration are expected with this breakup model.

Acknowledgments

The financial support by the Finnish Funding Agency of Technology and Innovation (Tekes) within the Cleen SHOK project Future Combustion Engine Power Plant (FCEP) is deeply acknowledged. The authors would like to thank the Finnish IT Center for Science (CSC) for providing the computational resources.

References

[1] F. X. Tanner. Liquid jet atomization and droplet breakup modeling of non-evaporating diesel fuel sprays. In *SAE World Congress*, Detroit, 1997. SAE Technical Paper 970050.

[2] F. X. Tanner and G. Weisser. Simulation of Liquid Jet Atomization for Fuel Sprays by Means of a Cascade Drop Breakup Model. In *SAE World Congress*, Detroit, 1998. SAE Technical Paper 980808.

[3] R. D. Reitz. Modeling atomization processes in high-pressure vaporizing sprays. *Atomisation and Spray Technology*, 3:309–337, 1988.

[4] Engine Combustion Network (ECN). "Spray A" Operating Condition, March 2012. URL `http://www.sandia.gov/ecn/cvdata/sprayA.php`.

[5] W. E. Ranz and W. R. J. Marshall. Evaporation from Drops, Part I. *Chemical Engineering Progress*, 48: 141–146, 1952.

[6] R. B. Bird, W. E. Stewart, and E. N. Lightfoot. *Transport Phenomena*. Wiley, second edition, 2002.

[7] V. Vuorinen, H. Hillamo, O. Kaario, M. Nuutinen, M. Larmi, and L. Fuchs. Effect of Droplet Size and Atomization on Spray Shape: A Priori Study Using Large-Eddy Simulation. *Flow, Turbulence and Combustion*, 86:533–561, 2011.

[8] P. J. O'Rourke and A. A. Amsden. The TAB Method for Numerical Calculation of Spray Droplet Breakup. 1987. SAE Technical Paper 872089.

[9] O. Kaario, M. Larmi, and F. X. Tanner. Non-Evaporating Liquid Spray Simulations with the ETAB and WAVE Droplet Breakup Models. In *ILASS-Europe*, Zaragoza, 2002.

[10] O. Kaario, H. Pokela, L. Kjäldman, J. Tiainen, and M. Larmi. LES and RNG turbulence modeling in DI diesel engines. In *SAE World Congress*, Detroit, 2003. SAE Technical Paper 2003-01-1069.

[11] S. Som and S. K. Aggarwal. Effects of primary breakup modeling on spray and combustion characteristics of compression ignition engines. *Combustion and Flame*, 157(6):1179 – 1193, 2010.

[12] N. Bharadwaj and C. J. Rutland. A Large-Eddy Simulation Study of Sub-Grid Two-Phase Interaction in Particle-Laden Flows and Diesel Engine Sprays. *Atomization and Sprays*, 20(8):673–695, 2010.

[13] OpenFOAM, December 2011. URL `http://www.openfoam.com`.

[14] F. F. Grinstein, L. G. Margolin, and W. J. Rider. *Implicit Large Eddy Simulation*. Cambridge University Press, 2007. ISBN 978-0-521-86982-9.